Available online at www.sciencedirect.com

ScienceDirect

Procedia CIRP 65 (2017) 70 – 77

www.elsevier.com/locate/procedia

3rd CIRP Conference on BioManufacturing

Material Removal Mechanisms in Grinding of Mixed Oxide Ceramics

Berend Denkena[a], Sarah Busemann[a], Lukas Gottwik[b], Thilo Grove[a], Andi Wippermann[a]*

[a]*Institute of Production Engineering and Machine Tools (IFW), Leibniz Universität Hannover, An der Universität 2, 30823 Garbsen, Germany*
[b]*CeramTec GmbH, CeramTec-Platz 1-9, 73207 Plochingen, Germany*

* Corresponding author. Tel.: +49-511-762-5953; fax: +49-511-762-5115. *E-mail address:* wippermann@ifw.uni-hannover.de

Abstract

The technological basis for a cost-effective and reliable grinding process of mixed oxide ceramics requires a fundamental understanding of the prevailing grinding mechanisms to maintain surface quality and strength requirements. However, these material removal mechanisms are not yet fully understood. This paper presents an innovative quick stop device for the interruption of cut during grinding. This appropriate method allows a detailed analysis of the interactions of grains along the contact zone. The results reveal correlations between the prevailing grinding mechanisms, the tetragonal to monoclinic phase transformation of the zirconia based ceramics as well as the resulting bending strength.

© 2016 The Authors. Published by Elsevier B.V. This is an open access article under the CC BY-NC-ND license
(http://creativecommons.org/licenses/by-nc-nd/4.0/).
Peer-review under responsibility of the scientific committee of the 3rd CIRP Conference on BioManufacturing 2017

Keywords: oxide ceramic, material removal mechanism, active abrasive grains, grinding

1. Introduction

Mixed oxide ceramics have found a widespread utilization in a variety of biomedical applications due to their favorable material properties. Especially, zirconia doped oxide ceramics possess an unusual combination of high strength and high fracture toughness. These characteristics are largely associated with the volume-increasing effect of the tetragonal-to-monoclinic phase transformation and its release during crack propagation. This feature is attributed to the stabilization of the metastable tetragonal phase through alloying with aliovalent ions, thus the tetragonal phase can revert to the stable monoclinic form [1,2].

Because of the hardness and brittleness of ceramics, grinding is the only method to generate required shapes. Comparing all conventional machining processes in common use, grinding is the most expensive per unit volume of material removal. In manufacturing of precision sintered ceramic components, grinding is the most significant portion of the total cost and can comprise up to 80 %. To meet the increasing demand of high performance ceramics, cost-effective grinding processes are needed [3-5].

Besides the grinding cost, a reliable process is highly relevant to maintain the required surface integrity, especially for components in the field of medical technology like implants. Lowering of processing costs by grinding with higher material removal rates can cause surface damage, which applies particularly for sensitively reacting ceramic materials. During grinding, the abrasive grains of the grinding wheel generate intense local stress fields upon contacting and penetrating the ceramic surface. Thus, a thin layer of the workpiece surface is exposed to high stress combined with high temperatures that cause irreversible material deformation in the form of dislocations and cracks. This grinding induced surface damage can lead to strength degradation or even to a catastrophic failure of the ceramic implant. The stress caused by the process can also trigger the tetragonal-to-monoclinic phase transformation, which is not reversible without a further heat treatment. However, the processes in the contact zone of grinding wheel and workpiece are not fully understood yet. [3-8].

In the past, most research on grinding mechanisms for ceramics has followed either the "machining" approach or the "indentation fracture mechanics" approach. The "indentation fracture mechanics" approach simplifies the grinding process by using a single indenter. It assumes that the damage produced

2212-8271 © 2016 The Authors. Published by Elsevier B.V. This is an open access article under the CC BY-NC-ND license
(http://creativecommons.org/licenses/by-nc-nd/4.0/).
Peer-review under responsibility of the scientific committee of the 3rd CIRP Conference on BioManufacturing 2017
doi:10.1016/j.procir.2017.04.011

by numerous abrasive grains during grinding can be modeled by the idealized flaw system caused by a sharp indenter. The “machining” approach typically includes the measurement of process variables like grinding forces combined with the examination of the resulting surface morphology [3,4].

This paper aims to close the gap between the two main research approaches by using an innovative quick stop device for the interruption of cut during the real grinding process without any simplifications. With this method, it is possible for the first time for grinding of ceramic to investigate the interaction of the numerous active abrasive grains that are engaged within the contact zone at the same time, each under different conditions. Furthermore, it is possible to relate the process parameters, e.g. grinding forces, to the number of active abrasive grains and not only to the area of the contact zone. With respect to the grinding forces, this provides a more reliable information about the stresses upon the workpiece during grinding. For the investigation of the prevailing material removal mechanisms and their influence on the resulting surface damage and mechanical properties of the oxide ceramic two different bond systems, namely resin and metallic bond, were used. In addition, the results reveal correlations between the prevailing grinding mechanisms, the monoclinic phase content of the zirconia based ceramic as well as the resulting residual stresses and the measured bending strength.

Nomenclature

v_c	cutting speed
v_f	feed velocity
a_e	depth of cut
h_{cu}	uncut chip thickness
d_g	diamond grain size

2. Experimental setup

2.1. Quick stop device

For the investigation of material removal mechanisms, quick stop experiments have frequently been used in the past to describe the interaction of the tool and the workpiece by interruption of cut during the machining process. Due to the abrupt interruption, the contact zone can be seen as a snap-shot of the current material removal mechanisms. The high cutting speed is the critical factor for reliable results of quick stop experiments especially in grinding. This is the reason why the first experiments deal with the interruption of cutting processes [9]. Later publications contain the interruption of abrasive processes. Buda and Liptak for example obtained several chip roots in up-grinding by using a self-developed segment acceleration method [10].

Lately Denkena et al. developed two different quick stop devices for the investigation of chip roots while grinding metals [11-13]. However, these approaches had disadvantages regarding the maximum grinding speed of only v_c = 5 m/s and an unsatisfactory repeatability. Therefore, a new design of a quick stop device was developed combining the advantages of the two quick stop devices used so far. The main requirements were a very strong external acceleration unit, a universal setup that can be used on almost every machine tool and a secure brake device to decelerate the guided sliding carriage with the ground sample. This challenge has already been technically demonstrated with success for interruption of grinding processes with cutting speeds up to v_c = 35 m/s [14].

This quick stop device was improved once again. The major improvements were a stronger captive bolt pistol and a higher stiffness of the whole setup to achieve results that are even more reliable. For this, all components of the quick stop device were manufactured out of hardened tool steel to reduce any deflection or slight unintended movements to a minimum. The new and stronger captive bolt pistol produces a kinetic energy of 384 J when applying the most powerful available cartridges [15]. This means an increase of the kinetic energy of nearly 40 % in comparison to the old captive bolt pistol (275 J) [14]. To achieve the maximum acceleration, the masses of the sliding carriage and the sample must be as low as possible without breakage at the moment of impact. The mass of the sliding carriage together with the mounted sample is 122.2 g. Measurements with a high-speed camera show that the sliding carriage reaches a maximum speed of 66 m/s after impact of the bolt that has a mass of 233.4 g.

Fig. 1 depicts an overview of the experimental setup and five detailed images of the main process sequences of the quick stop experiment. The overview shows the entire quick stop device fastened on a single base plate that is mounted on the machine bench of a Röders RFM 600 machine tool. The main parts of the device are the captive bolt piston, the dovetail guidance, the sliding carriage with the sample and two brake devices. The first step of the process sequence is a pre-grinding process of the mounted sample to ensure the adjusted process conditions in the following quick stop experiment (Fig. 1a). A shear pin within the precision dovetail guidance fixes the sliding carriage. An additional screw produces a preload to avoid any movement. After pre-grinding, a metal cable is connected to the infeed axis to trigger the bolt in the upcoming quick stop experiment (Fig. 1b). The metal cable works like an automatic releaser that triggers the bolt in every experiment at identic time and position of the grinding wheel on the workpiece regardless of the feed velocity v_f. After triggering the bolt, it accelerates the sliding carriage due to the impact opposite to the feed rate direction into brake I (Fig. 1c). Brake I consists of a metal enclosure with an interior technical high-density foam absorbing the high kinetic energy of the sliding carriage. It may occur that the sliding carriage moves back to the grinding wheel because of expanding of the compressed foam. For this reason, a second break II moves out when the sliding carriage leaves its initial position to avoid a renewed contact with the grinding wheel after the interruption of cut (Fig. 1d). At the end of the experiment the sliding carriage stops between brake I and brake II (Fig. 1e).

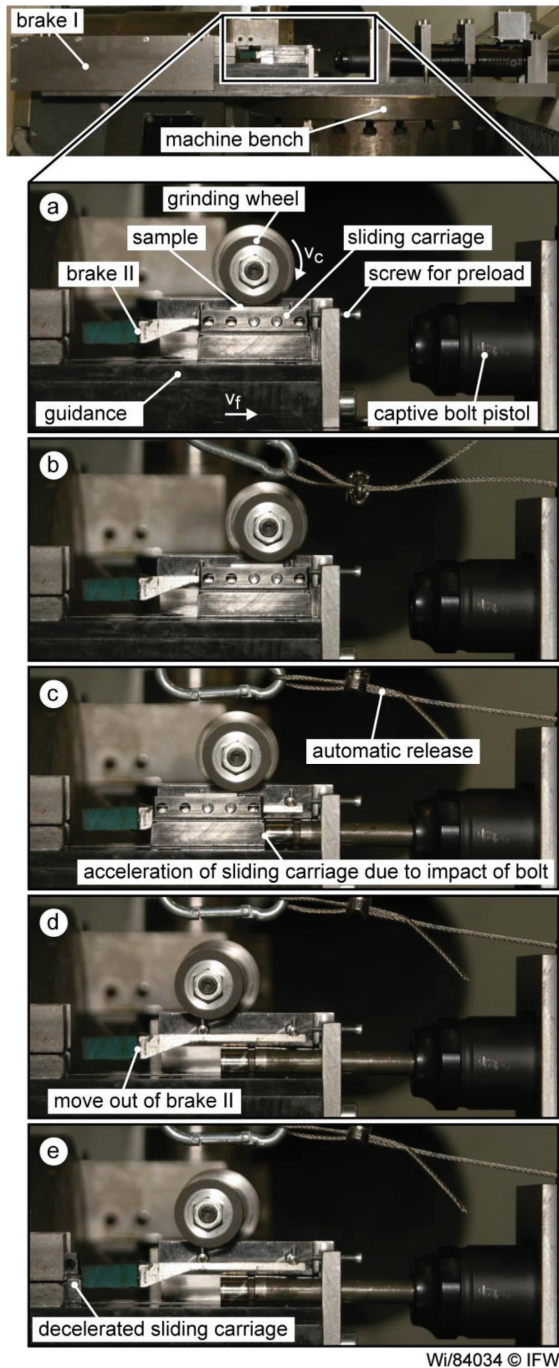

Fig. 1. Setup and process sequence of the quick stop experiment.

2.2. Grinding experiments

For this series of experiments the grinding process was conducted as a standard face grinding operation in up-grinding mode. Table 1 summarizes the parameter settings of the grinding experiments. In this study all process or output variables are referred to the uncut chip thickness h_{cu}, because this value obtains the manipulated input variables as well as the system variables regarding the grinding tool. For the calculation of the uncut chip thickness the approach of Lierse is used [24].

Subsequently, the ceramic workpieces are analyzed via SEM (Zeiss EVO 60 VP) to determine the prevailing material removal mechanisms and to count the number of active abrasive grains in the contact zone.

Table 1. Face grinding - parameter setting.

Process parameter					
Cutting speed v_c [m/s]			30		
Feed velocity v_f [mm/min]	100	3100	6100	9100	12100
Depth of cut a_e [mm]			0.1		
Bond	Resin or metal bond				
Coolant	5 % oil-in-water emulsion				

The entire examination was repeated without interruption of the grinding process. For this second series of experiments, it was possible to measure process forces during grinding as well as the monoclinic phase content, the resulting residual stresses and the bending strength of the ceramic workpieces after grinding. The process forces are measured via a Kistler 9257B piezoelectric 3-component dynamometer. Analysis of the monoclinic phase content and the near surface residual stresses (in direction of the feed motion) are determined applying the $\sin^2 \psi$-method using a GE XRD 3003 ETA X-ray diffraction system with a 2 mm diameter collimator and CoKα-radiation. Finally, the residual bending strengths σ_f are determined in a four-point bending test according to the standard DIN EN 843-1. The dimensions of the samples are 3 x 4 x 45 mm and the distances between the bearings are 40 mm for the lower ones and 20 mm for the upper bearings. The feed speed is 3.5 mm/min and the room is fully air-conditioned with a temperature of 24°C and an air humidity of 50 %.

2.3. Grinding tools

Grinding wheels with two different bond systems, namely resin bond and metal bond, are applied. Both grinding wheels have a 1A1-geometry and contain diamonds as abrasive grain material with a grain size of $d_g = 91$ µm. Both grinding wheels have a comparable high grain concentration of C176 (metal bond) and C150 (resin bond).

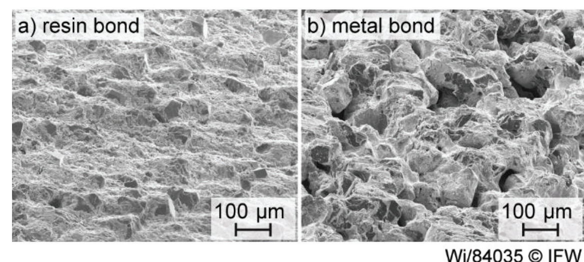

Fig. 2. (a) Micrograph of the resin and (b) metal-bonded grinding wheel topography.

The main differences between the bonding systems are their porosity and flexibility. The used metal bond has a high porosity that improves coolant supply (Fig. 2b) but a low flexibility in contrast to the resin bond with no porosity (Fig. 2a) but a higher flexibility. For grinding ceramics, these two bond systems are most commonly used. The choice of the grinding tool has a large influence on the development of the ground surface. Luthardt et. al. even assume that the grinding tool is the major factor for grinding induced surface damage [16].

2.4. Material

The material used in this study is a newly developed zirconia based mixed oxide ceramic by CeramTec GmbH, Germany. The matrix phase is 2 mol.% yttria-stabilized zirconia and the secondary phase is 5 vol.% dispersed strontiumhexaaluminate ($SrAl_{12}O_{19}$). Table 2 gives an overview about the mechanical properties at room temperature. It can be seen that the oxide ceramic exhibits a very high bending strength σ_f in combination with high fracture toughness K_{1c}. One of the reasons for this high fracture toughness is the secondary phase. Becher provide a fracture-mechanical explanation for the strengthening mechanisms known as crack deflection [25].

Table 2. Mechanical properties of the analyzed zirconia-based oxide ceramic.

Mechanical properties	
Bending strength σ_f [MPa]	1500-1800
Fracture toughness K_{1c} [MPa·√m]	8.8
Young's modulus [GPa]	213
Hardness HV10 [GPa]	12.6
Density ρ [g/cm³]	5.96

The mechanical properties listed in table 2 were determined according to the standards DIN EN 843 (four-point bending strength σ_f, young's modulus and hardness HV10), ISO 14627 (fracture toughness K_{1c}) and DIN EN 623-2 (density ρ).

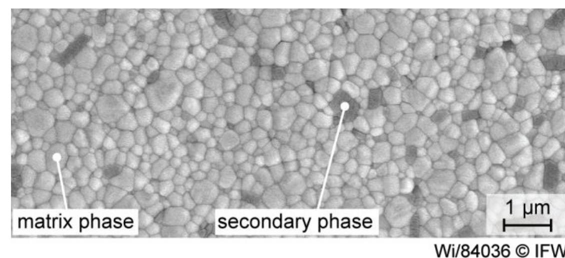

Fig. 3. Microstructure of the analyzed zirconia-based oxide ceramic.

Furthermore, the material has a microstructure with an average zirconia grain size of 0.27 ± 0.016 µm (Fig. 3). The zirconia grains are roundly in contrast to the plate-like strontiumhexaaluminate grains with an average size of 0.21 ± 0.035 µm. Due to the stochastic orientation of the strontiumhexaaluminate grains in the matrix phase, the cross section (Fig. 3) cannot represent the plate-like shape quite well. The micrograph is taken via SEM (Hitachi S-4700 II).

3. Results and discussion

3.1. Grinding wheel topography

At the beginning of the investigation the grinding wheels are dressed and sharpened. In order to generate a geometrically defined shape a form roller is used for dressing the metal-bonded grinding wheel whereas a SiC-dressing wheel is applied for dressing the resin-bonded tool. After the sharpening with a corundum sharpening block the wheel topographies are measured via a Mahr LD 130 profile and contour measuring device to determine the number of abrasive grains N_{GA} (z_s) in dependence of the grain depth z_s.

Due to the lower abrasion-resistance, the resin-bonded wheel shows more individual grains after setting back the bonding during sharpening (Fig. 4a). In contrast, the metal-bonded wheel has not that well exposed grains that are partially still covered with the bonding (Fig. 4b and Fig. 2b).

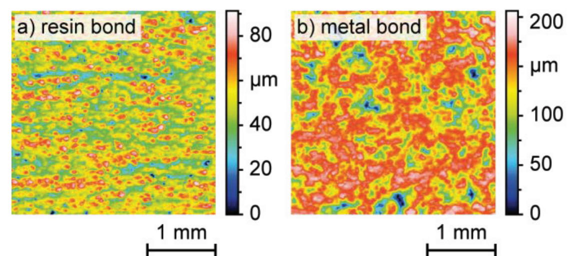

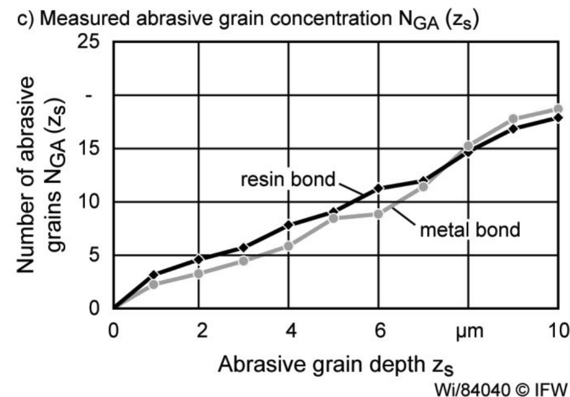

Fig. 4. (a) Measured topography and abrasive grain concentration depending on the grain depth of the resin and (b) metal-bonded grinding wheel.

In combination with the high porosity of the metal bond this is the reason why the resin-bonded wheel has a higher number of abrasive grains up to a grain depth of 7 µm, although the metal-bonded wheel has a higher grain concentration (Fig. 4c). This is the depth of the active abrasive grains of the grinding wheel below the surface where the highest abrasive grain in the bond is taken as the datum. It can be expected that the number of abrasive grains N_{GA} (z_s) of the resin bond is even higher during grinding, because of its flexibility.

3.2. Active abrasive grains

The number of active abrasive grains is counted by analyzing the micrographs of the contact zone after interruption of cut. The criterion for an active grain is a change of the homogeneous grinding grooves within the contact zone. Depending on the abrasive grain depth in the bond, the position of the grain within the contact zone at the moment of interruption and the chosen process parameter, the active grains leave different marks. Mainly, the active grains become visible as grooves or scratches that begin and/or end within the contact zone. At slower cutting speeds v_c they even leave material accumulations, which were in front of them at the moment of interruption (Fig. 5).

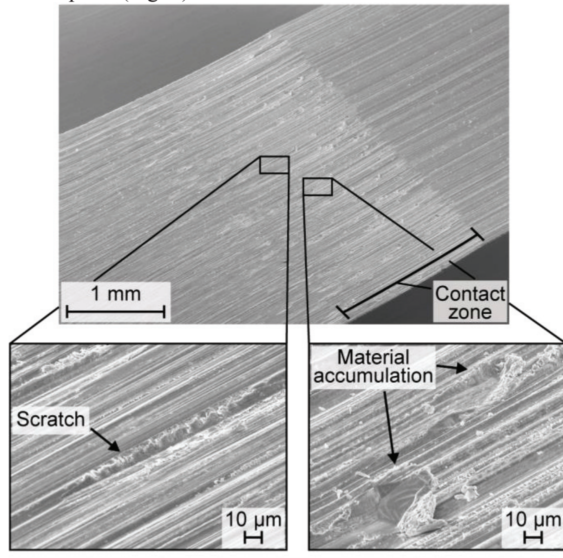

Fig. 5. Micrograph of the contact zone for analysis of active abrasive grains.

The number of active abrasive grains is divided by the area of the contact zone to get the number of active grains per square millimeter of each tool. The higher flexibility of the resin bond in combination with the higher concentration of abrasive grains N_{GA} (z_s) leads to more active grains within the contact zone.

For an increasing uncut chip thickness h_{cu} due to higher feed velocities v_f the number of active grains rises from over 14 up to 17 grains per square millimeter for the resin-bonded wheel. In contrast, the metal bonded wheel has an amount of active grains between 10 and 14 grains per square millimeter (Fig. 6). Besides the flexibility of the bond, the ductile material deformation is the reason for the higher number of counted abrasive grains (Fig. 6) in contrast to the static number of grains determined via evaluating the grinding wheel topography (Fig. 4).

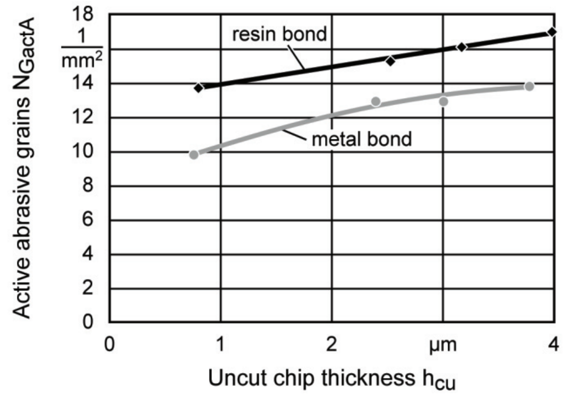

Fig. 6. Active abrasive grains per square millimeter of the resin and metal bonded grinding wheel.

3.3. Material removal mechanisms

In addition to the number of active grains, the prevailing material removal mechanisms are analyzed by evaluating the micrographs of the contact zone. For this, the contact zone is divided into three different sections. The criterion for the first section is a ductile formed grinding groove without any outbreaks (Fig. 7, yellow marked area). The criterion for the third section is a brittle erosion of the ceramic with mostly inter-crystalline outbreaks (red marked area). All areas that cannot be clearly allocated to the first or third section belong to the transition zone, which represents the second section. Scratches with chipping and material pieces dug out by fracture characterizes this section.

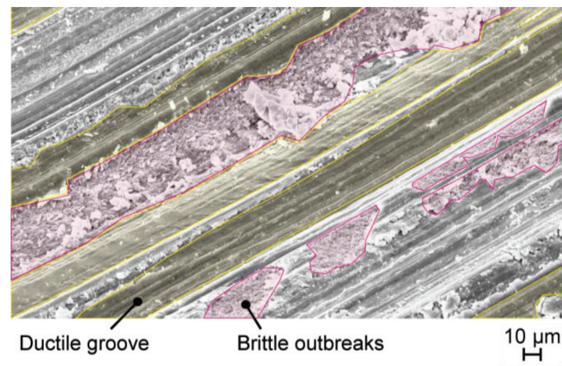

Fig. 7. Micrograph of an analyzed area of the contact zone for determining the prevailing material removal mechanisms.

Based on this approach, all parameter settings of both grinding wheels are evaluated. Fig. 8 summarizes the relation of the prevailing material removal mechanisms for an increasing uncut chip thickness.

Investigations of single-grain-scratches in brittle materials have demonstrated that below a certain scratching normal force the workpiece surface show crack-free and plastically deformed scratching traces. At higher uncut chip thickness values directly after the scratching process load relief cracks break open in the area behind or beside the abrasive grain due to residual tensile stresses and increasingly lead to brittle material erosion [17]. In principle, the conclusions can be transferred to the grinding process, where a large number of active abrasive grains is engaged [18].

It is remarkable that the ground zirconia-based ceramic shows a large proportion of ductile material removal even for higher uncut chip thicknesses. The amount of brittle breakouts is comparably low.

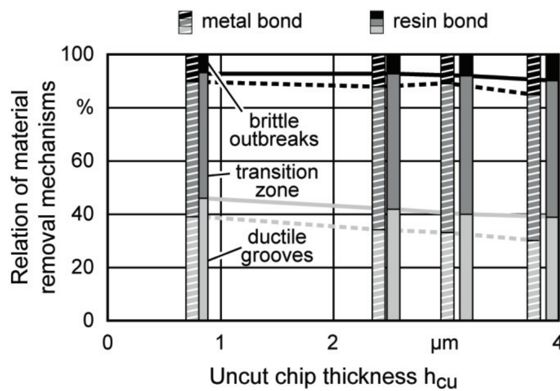

Experimental setup:
Cutting speed v_c = 30 m/s
Feed velocity v_f = var.
Depth of cut a_e = 0.1 mm

Grinding tools:
Abrasive: D91
Bond/grain concentration: resin/C150; metal/C176

Wi/84044 © IFW

Fig. 8. Relation of the prevailing material removal mechanisms.

Comparing both tools, the resin-bonded wheel shows a higher amount of ductile material removal between 39 % and to 46 %. For the metal-bonded wheel, the amount of ductile removed material is on average 10 % lower, but the amount of brittle outbreaks is on average 4 % higher. The higher amount of ductile material removal of the resin-bonded wheel can be explained not only by the grinding forces. It is assumed that also different thermal stresses during grinding or the different flexibility of the bonding system has an influence on the prevailing material removal mechanisms.

3.4. Process forces

Although the specific grinding forces in normal and tangential direction are apparently slightly higher for the resin-bonded grinding wheel, the grain grinding forces are lower (Fig. 9). The difference between the grain grinding forces of the resin- and the metal-bonded grinding wheel increases for

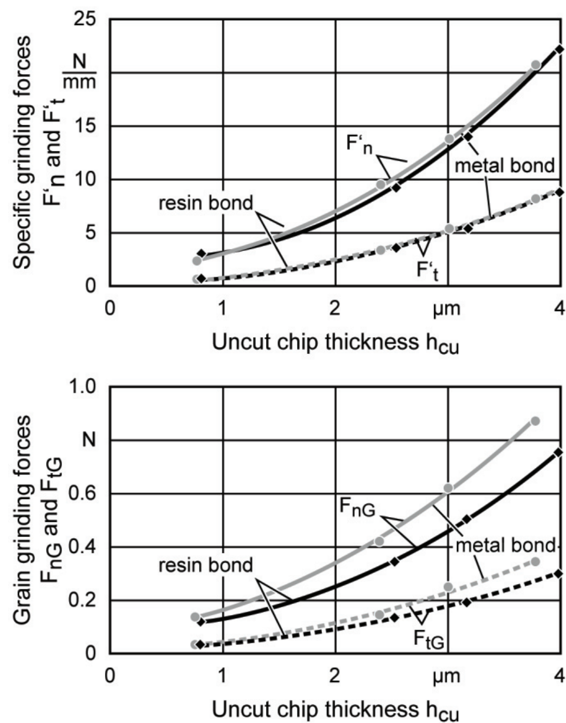

Experimental setup:
Cutting speed v_c = 30 m/s
Feed velocity v_f = var.
Depth of cut a_e = 0.1 mm

Grinding tools:
Abrasive: D91
Bond/grain concentration: resin/C150; metal/C176

Wi/84041 © IFW

Fig. 9. Specific grinding and grain grinding forces.

higher uncut chip thicknesses. Due to knowledge of the number of active abrasive grains per square millimeter, it is possible to relate the measured forces to this number of active grains and consequently to the contact point where the forces really arise. With this approach, the information on grinding forces is more reliable in comparison to the simple relation to the contact zone.

3.5. Bending strength analysis

During grinding, the abrasive grains of the grinding wheel generate intense local stress fields upon contacting and penetrating the ceramic surface. With a high number of active abrasive grains the introduced stress is distributed more evenly to a larger contact area. This means a reduced risk of surface damage in the form of dislocations and cracks that can lead to strength degradation of the sensitively reacting ceramic. Fig. 10 summarizes the results of the four-point-bending tests of the ground ceramic bending bars for both bond systems. Each data point is the mean value of five repetitions. Standard deviations are also given.

The bending strengths are comparable for both grinding wheels when applying small uncut chip thickness values. For increasing uncut chip thicknesses and corresponding higher

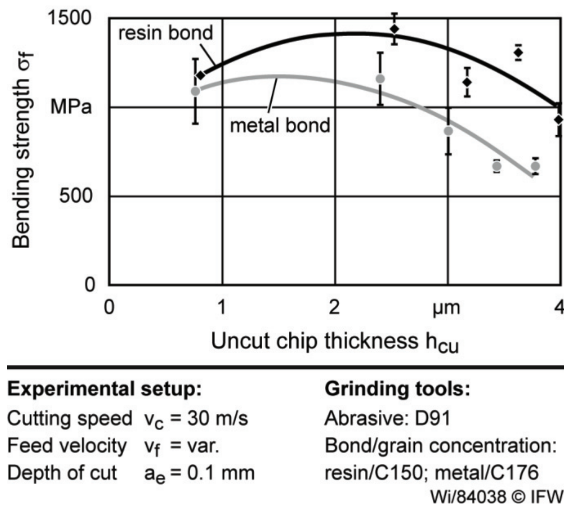

Fig. 10. Residual bending strength of the ground ceramic.

mechanical loads during grinding a strength degradation occurs for both bond systems. But this degradation is shifted to higher uncut chip thicknesses when using the resin-bonded grinding wheel. Furthermore, the maximum bending strength of 1443 MPa is more than 24 % higher than the measured maximum bending strength of the ground bending bars processed by the metal-bonded grinding wheel (1160 MPa).

3.6. Residual stresses measurement and phase analysis

The increase and the following degradation of the measured bending strength correlate with the determined residual stresses (Fig. 11). For the resin-bonded grinding wheel only compressive residual stresses between - 291 MPa and - 599 MPa are measured. The compressive residual stresses increase with increasing uncut chip thicknesses up to h_{cu} = 3.62 µm. For the highest uncut chip thickness a decrease of bending strength is observed. In contrast, the residual stresses of workpieces ground by the metal bonded grinding wheel show comparable values for small uncut chip thicknesses, but a large decrease for an uncut chip thickness higher than h_{cu} = 2.4 µm. For the two highest uncut chip thickness values even tensile residual stresses up to 129 MPa are measured.

Grinding with increasing uncut chip thicknesses leads to increasing crack depth and reduced strength [19]. On the other hand, it can also lead to increasing compressive residual stresses, which means a strengthening effect for the ceramic workpiece. The compressive residual stresses are a consequence of micro-plastic deformation during grinding and the phase transformation to the monoclinic structure [19,21,22]. This phase transformation is linked to a volume increase of about 4 % that causes a compression zone near the precipitate [22].

In this context, Fig. 11 depicts the corresponding monoclinic ZrO_2-phase content that is comparable for the smallest uncut chip thickness regardless of the grinding tool. The phase content is calculated by the ratio of the peak intensities of the two monoclinic peaks ($I_m(111)$, $I_m(11\bar{1})$) as well as the tetragonal peak ($I_t(111)$) [23]. For an increasing uncut chip thickness the monoclinic phase content remains almost constant in case of using the resin-bonded grinding wheel, but decreases significantly after grinding with the metal-bonded tool.

The monoclinic phase content is one of the reasons for the higher residual compressive stresses and consequently for the higher bending strength of the workpieces ground by the resin-bonded grinding wheel. Another explanation for the lower bending strength of samples ground by metal-bonded tool might be the higher crack depth. Cracks are found on all micrographs, but an information about their depth is missing. The depth of cracks and the thickness of the surface layer containing compressive residual stresses are competitive effects regarding the resulting bending strength [20]. A further explanation can be a pronounced thermal influence of the grinding process in case of the determined tensile stresses using the metal-bonded tool, although it has a high porosity that improves coolant supply [21]. The secondary phase is chemically stable and shows no transformation due to the grinding process.

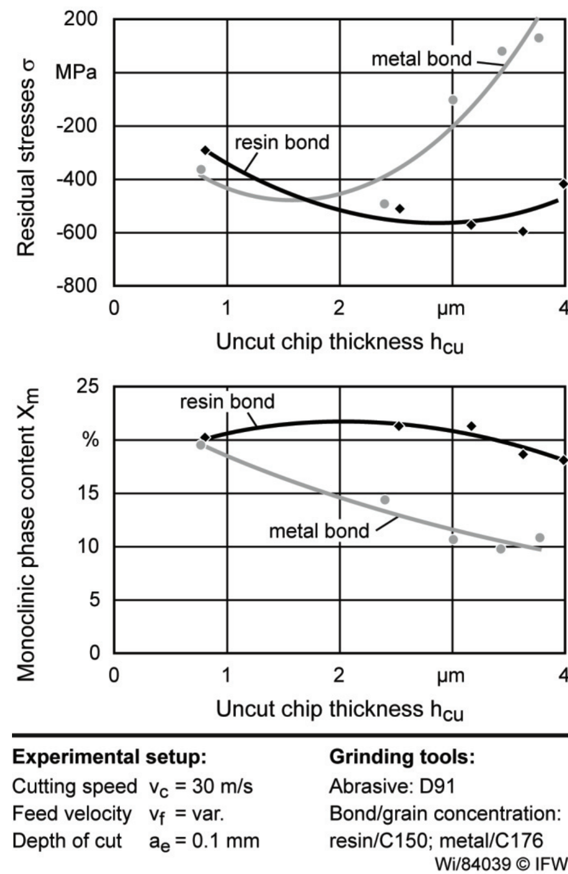

Fig. 11. Residual stresses and monoclinic ZrO_2-phase content of the ground ceramics.

4. Conclusion

The development of new zirconia-based oxide ceramics with outstanding mechanical properties is leading to their more widespread consideration for medical applications. However, actual utilization of high strength ceramics has been limited mainly by the grinding costs and the need to ensure the required surface integrity. Especially for components in the field of medical technology like implants, it is highly relevant to maintain the required bending strength. Therefore, a fundamental understanding of the grinding process is needed.

To analyze the prevailing material removal mechanisms an innovative quick stop device for the interruption of cut during grinding was deployed successfully. By means of this method it has been shown that the resin-bonded grinding wheel leads to a higher amount of ductile material removal during grinding. One of the reasons is the higher number of active abrasive grains within the contact zone. It has been demonstrated that the grinding tool and especially the number of active abrasive grains has a large impact on the resulting bending strength of the ground workpiece. Due to more active grains a more even distribution of the introduced stress to a larger contact area is achieved. Consequently, the grain grinding forces are lower for the resin bonded grinding wheel, which means a reduced risk of grinding induced surface damage and strength degradation.

Subsequently, the determined bending strength behavior for increasing uncut chip thickness has supported this statement. Furthermore, the bending strength correlates with the observed residual stresses as well as with the content of monoclinic phase. The larger decrease of bending strength at a lower level in case of using the metal-bonded tool can be explained with tensile residual stresses and a comparable low monoclinic phase content. Besides the introduced grinding forces, the thermal stress during grinding should have a large influence on the decrease of bending strength. This influence is part of the following investigations.

From these results, recommendations regarding the tool choice as well as the grinding settings have been derived aiming for an improved grinding process by maintaining the required strength of the new developed oxide ceramic.

Acknowledgements

The authors would like to thank the German Research Foundation (DFG) for supporting the subproject T5 within the Collaborative Research Center 599 “Sustainable bioresorbable and permanent implants of metallic and ceramic materials”.

References

[1] Garvie RC, Hannink RH, Pascoe RT. Ceramic Steel?. Nature 1975; 258:703-4.
[2] Chevalier J, Gremillard L, Virkar AV, Clarke DR. The Tetragonal-Monoclinic Transformation in Zirconia: Lessons Learned and Future Trends. Journal of The American Ceramic Society 2009;92(9):1901-20.
[3] Malkin S, Hwang TW. Grinding Mechanisms for Ceramic. Annals of the CIRP 1996;45(2):569-80.
[4] Malkin S, Ritter JE. Grinding Mechanisms and Strength Degradation of Ceramics. Key Engineering Materials 1992;71:195-212.
[5] Kitajima K, Cai GQ, Kumagai N, Tanaka Y, Zheng HW. Study on Mechanisms of Ceramic Grinding. Annals of the CIRP 1992;41(1):367-71.
[6] Zhang B, Zheng XL, Tokura H, Yoshikawa M. Grinding induced damage in ceramics. Journal of Materials Processing Technology 2003;132:353-64.
[7] Zhang B, Howes TD. Material-Removal Mechanisms in Grinding Ceramics. Annals of the CIRP 1994;43(1):305-8.
[8] Krishnamurthy R, Arunachalam LM, Gokularathnam CV. Grinding of Tranformation-Toughened Y-TZP Ceramics. Annals of the CIRP 1991;(1):331-3.
[9] Furrer JC, Dinichert P. Vorrichtung zur plötzlichen Schnittunterbrechung. Fertigung 1974;5(3):105-8.
[10] Buda J, Liptak J. Grinding mechanism investigation based on winning and evaluation of chip roots. Journal of Mechanical Working Technology 1988;17:157-65.
[11] Denkena B, Köhler J, Kästner J. Chip formation in grinding: an experimental study, Production Engineering Research and Development (WGP) 2012;2(2):107-15.
[12] Denkena B, Grove T, Seiffert F. Mikrogeometrische Eingriffsverhältnisse beim Längsumfangsplanschleifen. Diamond Business 2015;52:62-72.
[13] Denkena B, Grove T, Seiffert F. Chip Roots analysis in peripheral longitudinal up-grinding by means of a new quick-stop device. International Journal of Abrasiv Technology 2015;7(1):59-72.
[14] Göttsching T, Wippermann A, Grove T. Quick Stop Device to Analyze the Chip Formation Mechanisms in Face Grinding. Advanced Materials Research 2016;1140:221-7.
[15] Dörfler K, Troeger K, Lautenschläger R, Lücker E. Bewertung verschiedener Bolzenschuss-Betäubungsapparate beim Rind. Mitteilungsblatt Fleischforschung Kulmbach 2013;52(200):113-24.
[16] Luthardt RG, Holzhüter MS, Rudolph H, Herold V, Walter MH. CAD/CAM-maching effects on Y-TZP zirconia. Dental Materials 2004;20:655-62.
[17] Roth P. Abtrennmechanismen beim Schleifen von Aluminium-oxidkeramik. Dr.-Ing. Dissertation 1994, Hannover.
[18] Tönshoff HK, Denkena B. Basics of Cutting and Abrasive Processes. Lecture Notes in Production Engineering 2013, Springer.
[19] Pfeiffer W, Hollstein T. Damage determination and strength prediction of machined ceramics by X-ray diffraction techniques. Machining of Advanced Materials 1993;45:235-45.
[20] Eigenmann B. Röntgenographische Analyse inhomogener Spannungszustände in Keramiken, Keramik-Metall-Fügeverbindungen und dünnen Schichten. Dr.-Ing. Dissertation 1992, Karlsruhe.
[21] Hessert R, Eigenmann B, Vöhringer O, Löhe D. Fracture mechanical evaluation of the effects of grinding residual stresses on bending strength of ceramics. Materials Science and Engineering 1997;A234-236:1126-9.
[22] Claussen N. Stress-Induced Transformation of Tetragonal ZrO2 Particles in Ceramic Matrices. Journal of The American Ceramic Society 1977;61:85-6.
[23] Surberg CH, Wuthnow H. Rötgenographische Analyse der ZrO_2-Polymorphen an Pulvern. Cfi/Ber. DKG 73 1996;11/12:674-7.
[24] Lierse T. Mechanische und thermische Wirkungen beim Schleifen keramischer Werkstoffe. Dr.-Ing. Dissertation 1998, Hannover.
[25] Becher PF. Microstructural design of toughened ceramics. Journal of American Ceramic Society 1991;74:255-69.